PAPER

Chemical imaging of microfluidic flows using ATR-FTIR spectroscopy

K. L. Andrew Chan,[a] Shelly Gulati,[bc] Joshua B. Edel,[bc] Andrew J. de Mello[b] and Sergei G. Kazarian[*a]

Elucidating the chemical composition of microfluidic flows is crucial in both understanding and optimising reactive processes within small-volume environments. Herein we report the implementation of a novel detection methodology based on Attenuated Total Reflection (ATR)–Fourier Transform Infra-Red (FTIR) spectroscopic imaging using an infrared focal plane array detector for microfluidic applications. The method is based on the combination of an inverted prism-shape ATR crystal with a poly(dimethylsiloxane)-based microfluidic mixing device. To demonstrate the efficacy of this approach, we report the direct measurement and imaging of the mixing of two liquids of different viscosities and the imaging and mixing of H_2O and D_2O with consecutive H/D isotope exchange. This chemically specific imaging approach allows direct analysis of fluid composition as a function of spatial position *without* the use of added labels or dyes, and can be used to study many processes in microfluidics ranging from reactions to separations.

Introduction

As microfluidic technology continues to demonstrate its tremendous potential as a fundamental analytical tool in the chemical and biological sciences, the need to develop new robust, fast and sensitive detection techniques for chemical species detection intensifies. These detection methods must consider and account for the physical realities of microfluidic flows such as reduced diffusion lengths, confined geometries, and planar substrates[1] whilst preserving or enhancing the rapid, high-throughput, and small volume benefits and the ease of use of microfluidic systems. Small volume detection within microfluidic systems is most commonly performed using optical methods. Their widespread adoption is unsurprising, since glass and polymers (the substrate materials of choice) are normally transparent in the visible, near-UV and near-IR regions of the electromagnetic spectrum and thus allow sample contained within to be probed *via* the absorption, emission or scattering of radiation. More specifically, fluorescence-based methods are the most prevalent due to the exquisite sensitivity and selectivity of emission spectroscopy.[2,3] Furthermore, much of the early interest in microfluidic systems was driven by the need to create high-throughput tools for nucleic acid analysis. Importantly, established methods for fragment sizing, sequencing and DNA amplification all incorporate fluorescent chemistries to facilitate detection, making their transferral to planar chip formats facile. However, an obvious disadvantage of fluorescence detection methods relates to the need to label molecules not containing an appropriate fluorophore. As a result, there has been interest in integrating label-free detection techniques with microfluidics.

Such techniques include infrared spectroscopic detection,[4–6] Raman spectroscopy,[7–9] and surface-enhanced Raman spectroscopy (SERS).[10,11] These techniques are advantageous for chemical analysis because they are label-free and have a broad applicability. However, these methods are usually less sensitive than fluorescence-based approaches because they are either absorption techniques or relay on inefficient Raman scattering and because several of them need detectors that are far less efficient than UV/vis detectors or because the absorptivity of the spectral features is low. Nevertheless, the inherent chemical specificity of vibrational spectroscopic methods and their quantitative nature are often essential for studies of many systems, such as flows in microfluidic devices. Recently, the application of Fourier transform infrared (FTIR) spectroscopic imaging to microfluidics has been proposed.[12] The possibility of obtaining chemical and spatial information from dynamic systems in microfluidics offers new opportunities in this field.

FTIR imaging using a highly sensitive multi-pixel detector or focal plane array (FPA) is recognised as a powerful material characterization method[13,14] and has been applied to a broad range of studies in the past decade. The main advantage of this imaging method is that while mid-IR spectra provide a wealth of chemical information, the thousands of detector pixels, each simultaneously measuring a spectrum from a specific location of the sample, provides the possibility of obtaining a chemical snapshot of a system in a matter of minutes or seconds.[15]

We have recently developed a number of applications utilising inverted prism-shape crystals in macro Attenuated Total Reflection (ATR) mode with optimised spatial resolution and fields of view.[16,17] Measurement in an ATR mode also has the significant advantage of overcoming one of the primary difficulties in FTIR spectroscopy, namely the strong absorption of water in the infrared region obscuring other weaker spectral bands of interest.[18] The ATR mode employs a high refractive index infrared transparent crystal to create an internal reflection where the infrared light interacts, as an evanescent wave, in the lower refractive index medium (the sample).[19] The depth of this

[a] *Department of Chemical Engineering, Imperial College London, South Kensington Campus, London, SW7 2AZ, United Kingdom. E-mail: s. kazarian@imperial.ac.uk; Tel: +44 (0)20 7594 5574*
[b] *Department of Chemistry, Imperial College London, Exhibition Road, South Kensington, London, SW7 2AZ, United Kingdom*
[c] *Institute of Biomedical Engineering, Imperial College London, Exhibition Road, South Kensington, London, SW7 2AZ, United Kingdom*

interaction is up to several micrometers from the surface of the crystal. This small but well defined pathlength provides the basis for quantitative analysis in aqueous solutions and is independent of the sample thickness. ATR-FTIR imaging has been shown to be a powerful research tool in the study of wet systems such as dissolution of pharmaceutical formulations in water,[18] ingression of water into tissue,[20] imaging of live cells in culturing media[21] and studies of protein crystallisation.[22] Previously we have demonstrated that it is possible to study dissolution of multiple pharmaceutical formulations in 5 separate channels made of poly(dimethylsiloxane) with ATR-FTIR imaging using optics that expand the field of view.[23] Here, we introduce an approach for obtaining chemical images of liquids flowing in microfluidic channels by using the surface of an ATR crystal as the base of the microfluidic device. ATR-FTIR spectroscopic imaging is demonstrated for a range of fluid flows in a microfluidic Y-mixer device.

Experimental

FTIR spectra were measured using a continuous scan spectrometer (Varian 7000 FT-IR) in conjunction with a large sample compartment chamber. Images were measured using a focal plane array detector containing 64×64 pixels. Accordingly 4096 spectra were measured during each image acquisition. Images were collected using 32 co-additions, an 8 cm^{-1} spectral resolution and a spectral range of $4000–900 \text{ cm}^{-1}$. The scanning time for each image under these conditions is approximately 50 seconds.

A 45° single bounce inverted ATR prism made of ZnSe (PIKE) with a 20 mm diameter sampling surface was mounted onto a lab-made manual stage to allow both imaging and mapping for the larger area measurements. A more detailed description of the combined imaging and mapping experimental setup can be found elsewhere.[17]

Microfluidic channels were moulded into a poly-(dimethylsiloxane) (PDMS) elastomeric substrate (Dow Sylgard 184) using an SU-8 master and standard soft lithographic fabrication methods.[24,25] The channels were enclosed by self-adherence of the structured PDMS layer with the ATR crystal surface. Additionally, a thin poly(methyl methacrylate), (PMMA) sheet was contacted with the upper (unstructured) surface of the PDMS substrate and screwed down onto the top plate of the ATR crystal. This provided sufficient pressure to form a strong seal between the structured PDMS and ATR surfaces and prevent leakage of fluid under the applied flow regime. The PMMA sheet was machined with holes coinciding with the inlets and outlet of the microfluidic device to allow access of poly(ethylene) tubing in holes punched into the PDMS layer. The fluidic channel pattern used allows introduction of two fluids *via* inlet reservoirs. The inlet channels subsequently unite at a 90 degree angle to form a single serpentine channel (Fig. 1). This channel consists of two 180 degree turns and eventually connects with the exit reservoir. All the channels are 1000 μm wide and 50 μm deep.

Precision syringe pumps (PHD 2000, Harvard Apparatus) are used to deliver reagent solutions at flow rates between 25 and 75 μl/hr using 1 ml gastight syringes (SGE, Europe Ltd). Deionised water, poly(ethylene glycol) and D_2O were used as
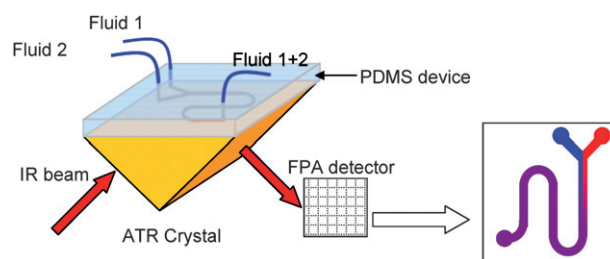

Fig. 1 Schematic diagram of ATR-FTIR imaging system and integration with a planer, chip-based microfluidic device.
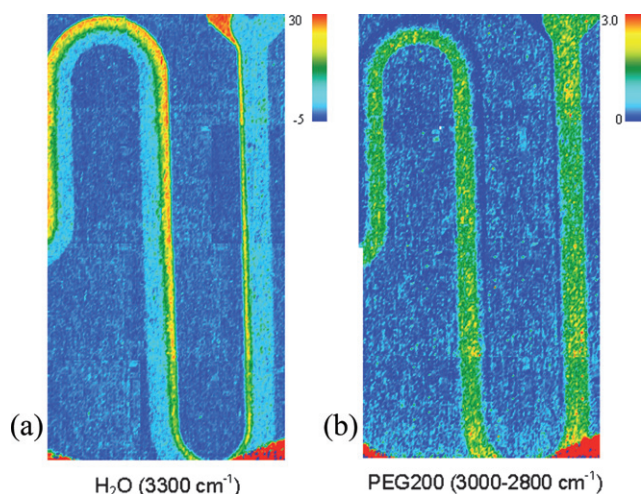
model fluids. Poly(ethylene glycol) and D_2O were both purchased from Sigma Aldrich.

Results and discussion

To demonstrate the feasibility of ATR-FTIR imaging of microfluidic flows, a simple Y-junction mixer (Fig. 1) is used herein. The microfluidic device footprint is essentially defined by the size of the ATR crystal. To date, the largest ATR crystal that has been used for imaging provides an image field of view of 15.4×21.4 mm.[12,23] However, realisation of such a large imaging area relies on the use of expanding optics which in turn significantly degrades the spatial resolution. An alternative way of obtaining a large field of view without sacrificing spatial resolution is to employ a combined imaging and mapping strategy. In such an approach, the ATR crystal (or internal reflection element) is translated to acquire an array of sub-images which can be reconstructed at a later time to generate the desired image. Indeed, this method has been used to capture the image of a latent fingerprint.[17] It should be noted that one disadvantage of the combined imaging and mapping strategy is that different sub-images are by definition measured at different points in time. Nevertheless, for a steady state system (such as a continuous microfluidic flow), this will not be a problem and an area of 10×14 mm² can be surveyed with a spatial resolution of approximately 40 μm in 15 minutes.[17]
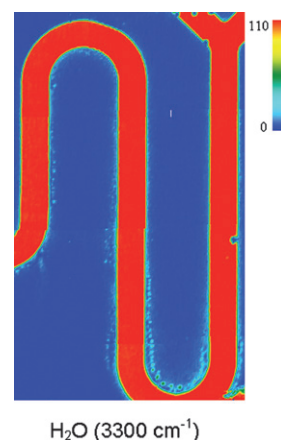
Fig. 2 ATR-FTIR image of a microfluidic channel containing water moving at a volumetric flow rate of 50 μl/hr from each input. Red indicates a high concentration of water whilst blue indicates a zero concentration of water. The overall imaged area is ~7.5 × 14 mm².
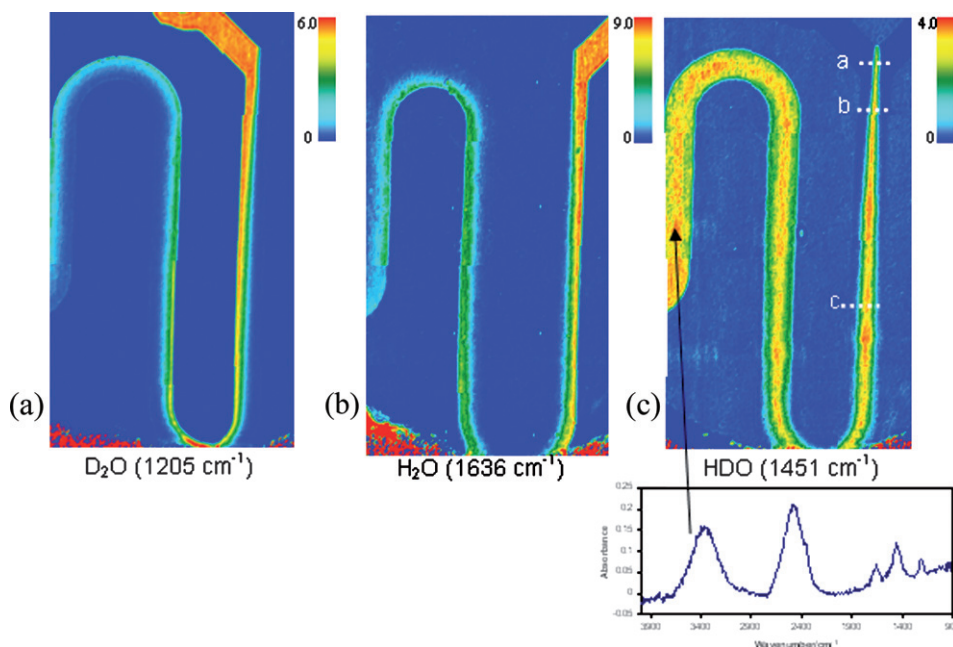
Fig. 3 ATR-FTIR images of the microfluidic device with water (left of the Y junction) and PEG200 (right of the Y junction) being introduced at flow rates of 75 and 25 µl/hr respectively. Images (a) and (b) illustrate the flow pattern of water and PEG 200 in the channel respectively. The overall imaged area is ∼7.5 × 14 mm².

integrated value of the area under the water ν(O–H) absorbance (3700–3100 cm⁻¹), with a straight base line connecting the limits of the integral, for each spectrum on the image plane. The image incorporates a false colour scale with red indicating a high relative concentration of water. The ATR-FTIR image of water closely matches the physical dimensions of the microfluidic channel, and also any defects generated during master generation.

Subsequent experiments were aimed at using ATR-FTIR to image fluidic mixing and reactive phenomena. Within microfluidic environments, laminar flow is typically prevalent (rather than turbulent flow) and mixing occurs by diffusion only. To demonstrate that such mixing processes can be probed using ATR-FTIR imaging, two miscible fluids, water and PEG200 were injected into each inlet of the microfluidic device. Specifically, a water stream is introduced *via* the left-hand branch of the Y junction whilst the PEG200 stream enters from the right. Since the viscosity of PEG200 is significantly higher than water, flow rates of 75 µl/hr for water and 25 µl/hr for PEG200 were used. Moreover, the system was allowed to equilibrate for approximately 10 minutes before the first image is captured. Two reconstructed ATR-FTIR images for this system are shown in Fig. 3. ATR-FTIR images were created using both the PEG specific ν(CH) absorption band (3000–2800 cm⁻¹) and the water ν(O–H) absorption band (3700–3100 cm⁻¹). The colours in Fig. 3 correspond to the absorbance of the absorption bands of water and PEG and are thus proportional to the concentrations of these substances, with red representing the highest concentration and dark blue representing zero concentration. Diffusion-based mixing of the two fluid streams can be clearly observed in both images, with the sharp boundary between the water and PEG200 flows at the point of confluence moving orthogonal to the flow direction and slowly become more blurred as a function of distance along the channel. The image of the distribution of PEG

In initial experiments, pure deionised water was pumped through the channel at a total flow rate of 100 µl/hr (50 µl/hr per input stream). ATR-FTIR images were recorded under flow once the channel was completely filled with water. Using the current experimental configuration, a single sub-image has dimensions of 2.6 × 3.6 mm. This is smaller than the active area of microfluidic device. Accordingly, the ATR crystal was x-y translated to acquire a total of 12 images (3 × 4 tiles) to build a full 7.5 × 14 mm² image. This reconstructed ATR-FTIR image is shown in Fig. 2. In this case, the image map is generated by plotting the

Fig. 4 ATR-FTIR images of the microfluidic device with D₂O (left of the Y junction) and water (right of the Y junction) being introduced at a flow rate of 50 µl/hr. Images (a), (b) and (c) illustrate the flow pattern of D₂O, H₂O and HDO in the channel respectively. The spectrum shown is extracted from the area indicated by the arrow. The overall imaged area is ∼7.5 × 14 mm².

in the channel close to the entry point (right hand side) in Fig. 3 may give the impression that the whole channel is fully occupied by PEG (because the volume of water is small). However, close inspection of the right image reveals that the left part of the channel is occupied by water which gradually diffuses into PEG. It can be seen that at the top of the second curve the space occupied by water and PEG are approximately the same with a clear gradient of concentration of water indicated by the gradient in colour. Importantly, this simple experiment demonstrates that the flow behaviour of multiple laminae within a microfluidic channel can be tracked *in situ* without the need to add any tracer molecules. Moreover, with the wealth of information contained in the mid-IR spectrum, multiple fluids can be simultaneously monitored in a single experiment.
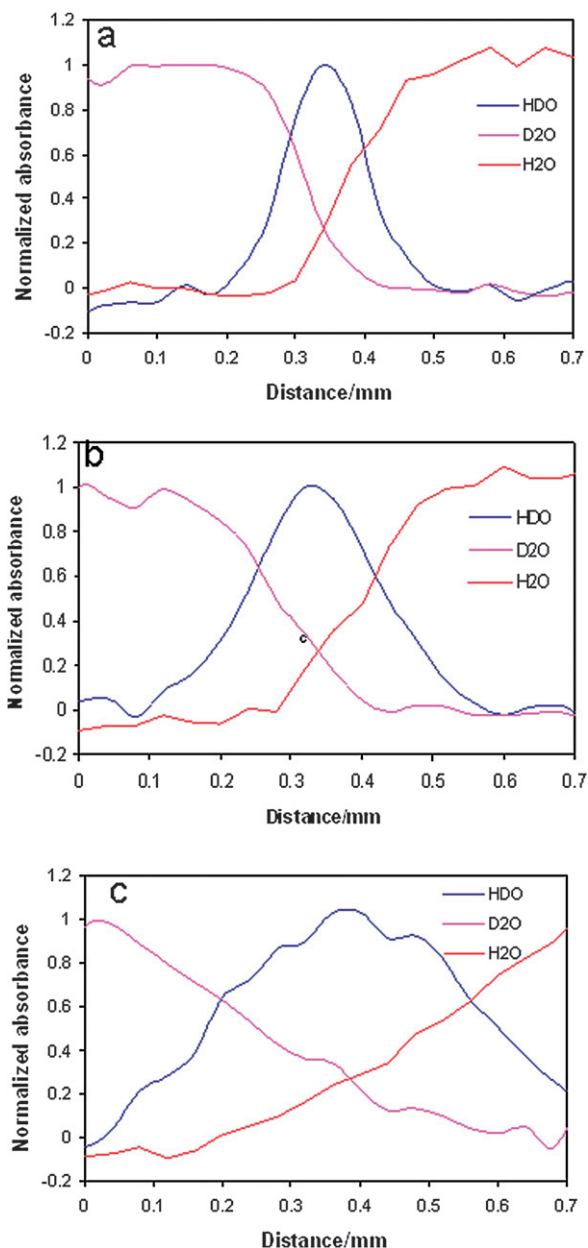
Fig. 5 Normalized absorbance profiles of D_2O, H_2O and HDO extracted along the white dotted lines shown in Fig. 4c.

In addition to the assessment of fluidic mixing within microfluidic channels, ATR-FTIR imaging can in principle be used to probe *in situ* chemical reactions. To demonstrate this facility, H_2O and D_2O streams were mixed within the microfluidic device at a total volumetric flow rate of 100 μl/hr. H_2O and D_2O undergo H/D isotopic exchange when they mix and form HDO. ATR-FTIR images of H_2O, D_2O and HDO are shown in Fig. 4. These images were measured simultaneously and spectra extracted from the input channels prior to confluence indicate that both D_2O and H_2O input streams are of high purity. Fluidic mixing can be evidenced by the blurring of the fluid interface as a function of distance along the microfluidic channel (Fig. 4a and b). Additionally, Fig. 4c demonstrates the formation of a new species subsequent to the confluence of the H_2O and D_2O streams. Spectra extracted from red regions in Fig. 4c illustrate two new bands at approximately 2500 and 1451 cm^{-1} representing the stretching and bending mode vibrations of HDO respectively. The ATR-FTIR image in Fig. 4c shows that HDO is formed initially at the interface between the D_2O and H_2O streams. Diffusion of this product orthogonal to the direction of flow occurs as expected as a function of distance along the microchannel. Spectral analysis of the material exiting the microchannel indicates a $D_2O:H_2O:HDO$ ratio of approximately 1:1:2. A key feature of ATR-FTIR spectroscopy is the ability to perform quantitative analysis. According to the Beer–Lambert law absorbance is proportional to concentration. Accordingly, absorbance profiles can be extracted from ATR-FTIR images and analysed quantitatively. Fig. 5 presents profiles extracted along the white dotted lines shown in Fig. 4c. These profiles indicate that reagent diffusion and reaction to form HDO progresses rapidly along the channel. The absorbance profiles of D_2O and H_2O intersect at the point where the normalised absorbance is approximately 30% of the maximum. This suggests that the reaction is fast and equilibrium is reached in a very short time. Moreover, it is interesting to observe (in Fig. 5a and b) that there are regions where the concentration of H_2O is close to zero while HDO is present. This observation is explained by the fact that the high concentration of D_2O means that D_2O molecules will react with the available water molecules and the amount of H_2O will depend on the equilibrium constant.

Conclusions

We have demonstrated that ATR-FTIR imaging can be used to chemically image multiple species flowing within microfluidic channels. This method can be used to study both mixing and reactions between fluids. Since ATR-FTIR imaging does not rely on the use of fluorescent or absorbing labels, all unexpected reactions can be observed and reaction products identified. The microfluidic channels used in the current experiments are relatively large in width. However, it should be noted that smaller dimensions can also be studied by implementation of different ATR accessories that provide better spatial resolution. For example we have previously shown that the use of a diamond ATR crystal can improve spatial resolution to between 10 and 15 μm. Additionally, although the current approach is ideal for studying steady-state (or continuous flow) systems, temporal resolution can be significantly increased to the millisecond range for analysing segmented flows by the implementation of step scan

technology.[26] Such developments will further enhance the applicability of this imaging technology in microfluidic studies. This powerful imaging technique affords label-free, high-throughput and quantitative analysis of a diversity of chemical and biological systems.

Acknowledgements

References

1 K. B. Mogensen, H. Klank and J. P. Kutter, *Electrophoresis*, 2004, **25**, 3498–3512.
2 E. K. Hill and A. J. de Mello, *Analyst*, 2000, **125**, 1033–1036.
3 O. Hofmann, G. Voirin, P. Niedermann and A. Manz, *Anal. Chem.*, 2002, **74**, 5243–5250.
4 Y. Xiao, X. D. Yu, K. Wang, J. J. Xu, J. Huang and H. Y. Chen, *Talanta*, 2007, **71**, 2048–2055.
5 T. Pan, R. T. Kelly, M. C. Asplund and A. T. Woolley, *J. Chromatography A*, 2004, **1027**, 231–235.
6 K. F. Jensen, *MRS Bulletin*, 2006, **31**, 101–107.
7 S. A. Leung, R. F. Winkle, R. C. R. Wootton and A. J. de Mello, *Analyst*, 2005, **130**, 46–51.
8 M. Lee, J. P. Lee, H. Rhee, J. Choo, Y. G. Chai and E. K. Lee, *Journal of Raman Spectroscopy*, 2003, **34**, 737–742.
9 J. B. Salmon, A. Ajdari, P. Tabeling, L. Servant, D. Talaga and M. Joanicot, *Applied Physics Letters*, 2005, **86**, 3.
10 G. L. Liu and L. P. Lee, *Applied Physics Letters*, 2005, **87**, 3.
11 F. T. Docherty, P. B. Monaghan, R. Keir, D. Graham, W. E. Smith and J. M. Cooper, *Chemical Communications*, 2004, 118–119.
12 S. G. Kazarian, *Anal. Bioanal. Chem.*, 2007, **388**, 529–532.
13 E. N. Lewis, P. J. Treado, R. C. Reeder, G. M. Story, A. E. Dowrey, C. Marcott and I. W. Levin, *Anal. Chem*, 1995, **67**, 3377–3381.
14 J. L. Koenig, S. Q. Wang and R. Bhargava, *Anal. Chem.*, 2001, **73**, 360A–369A.
15 C. M. Snively, S. Katzenberger, G. Oskarsdottir and J. Lauterbach, *Opt. Lett.*, 1999, **24**, 1841–1843.
16 K. L. A. Chan, F. H. Tay, G. Poulter and S. G. Kazarian, *Appl. Spectrosc.*, 2008, **62**, 1102–1107.
17 K. L. A. Chan and S. G. Kazarian, *Appl Spectrosc.*, 2008, **62**, 1095–1101.
18 S. G. Kazarian and K. L. A. Chan, *Macromolecules*, 2003, **36**, 9866–9872.
19 N. J. Harrick, *Internal reflection spectroscopy*, Harrick Scientific Corporation, New York, 1987.
20 S. G. Kazarian and K. L. A. Chan, *Biochim. Biophys. Acta.-Biomem.*, 2006, **1758**, 858–867.
21 M. K. Kuimova, K. L. A. Chan and S. G. Kazarian, *Appl. Spectrosc.*, 2009, **63**, 164–171.
22 K. L. A. Chan, L. Govada, R. M. Bill, N. E. Chayen and S. G. Kazarian, *Anal. Chem.*, 2009, **81**, 3769–3775.
23 K. L. A. Chan and S. G. Kazarian, *Lab on a Chip*, 2006, **6**, 864–870.
24 N. P. Beard, C.-X. Zhang and A. J. de Mello, *Electrophoresis*, 2003, **24**, 732–739.
25 D. C. Duffy, J. C. McDonald, O. J. A. Schueller and G. M. Whitesides, *Anal.l Chem.*, 1998, **70**, 4974–4984.
26 H. Sugiyama, J. Koshoubu, S. Kashiwabara, T. Nagoshi, R. A. Larsen and K. Akao, *Appl. Spectrosc.*, 2008, **62**, 17–23.